Master's thesis

Ultra-short pulse time domain Radar Cross Section measurements

W.A. van Cappellen

Date: July 13, 1998.
Supervisor: Prof.dr.ir. L.P. Ligthart.
Mentor: Ir. R.V. de Jongh.
Document number: 68–220–A256–98.

Delft University of Technology,
Faculty of Information Technology and Systems,
Department of Electrical Engineering,
Laboratory for Telecommunication and Remote Sensing Technology,
Mekelweg 4,
2628 CD, Delft,
The Netherlands.

Abstract

This report describes the feasibility and implementation of a time domain facility for Radar Cross Section (RCS) measurements. Main advantages of measuring in the time domain are the high range resolution and the application of direct gating. The limited signal to noise ratio can be a disadvantage.

The measurements have been performed with a sampling oscilloscope, a pulse generator and two 2–12 GHz ridged horn antennas. Because the horns are not designed for transmitting transient signals, an additional system response measurement in combination with a software deconvolution algorithm restores the impulse response of the object under test. Further processing separates the object response from clutter contributions.

A comparison of the time domain data with calculated and measured frequency domain radar cross sections shows a good agreement. The high range resolution enables the separation of scattering mechanisms (i.e. reflection, single and multiple diffraction). It is concluded that the time domain RCS measurement system is an attractive alternative of its frequency domain equivalent. However, the decision to measure in the time or frequency domain will depend on the specific aim of each experiment.

Acknowledgements

Many people have contributed to the realisation of this MSc. project. First of all I would like to mention my mentor René de Jongh. He teached me how to survive in the time domain and shared all his time domain measurement experiences. He made me realise and appreciate the unique features of the facilities. Thank you very much.

I would also thank Alex Yarovoy for his very interesting discussions and critical reading of this report. I am also very grateful to Peter Swart, a frequency domain RCS expert, for his technical suggestions and the availability of the object. I would also like to thank J.H. Zijderveld for his assistance during the preparation of the measurements. I would like to express special thanks to Lucas van Ewijk (TNO–FEL) for his introduction in scattering phenomena last year, his experience, the RCS predictions and his position in my graduation committee. I want to thank all IRCTR members who are not mentioned here for providing me a pleasant atmosphere, many suggestions and support.

Last but not least I would like to express my appreciation for Professor Ligthart for his critical, but very encouraging, attitude.

Contents

List of Figures

Chapter 1

Introduction

This report describes the feasibility and implementation of a time domain facility for Radar Cross Section (RCS) measurements. RCS measurements have a large number of applications, ranging from model verification to a powerful design tool for ships and aircraft.

RCS measurements are usually performed in the frequency domain. The International Research Centre for Telecommunication -transmission and Radar (IRCTR) already operates such frequency domain facilities. Recently IRCTR extended its facilities to perform ultra-short pulse antenna time domain measurements beyond its conventional frequency domain setup [1], [2]. These measurements successfully demonstrated the advantages and potentials of the time domain alternative [3].

Application of the time domain equipment in scattering research could also be very beneficial. Shorter measurement times could reduce the load on scarce measurement facilities and with the high range resolution scattering sources are easily identified. Time domain scattering measurements can also be used to estimate the maximum RCS of an object in a wide range of frequencies (e.g. when performing out-of-band antenna measurements).

The main topics of this thesis are:

- **Antenna selection**.

  Transmitting an ultra-short pulse requires specially designed transient antennas. What antennas should be used for scattering measurements?

- **Signal to noise ratio**.

  The signal to noise ratio of ultra-short pulse measurements is relatively low compared to the frequency domain equivalent. Does the pulse contain sufficient energy to perform scattering measurements?

- **Analysis of the measurement results.**

  What is the relation between the measured response and the object? What object characteristics can be obtained from the time domain measurements?

This thesis report starts with a short introduction in RCS and electromagnetic scattering theory. In section 3 the advantages and limitations of RCS measurements in the time domain are described. The error sources in time domain measurements are described in section 4. Section 5 contains a detailed description of the measurements. The next chapter describes the function and implementation of the signal processing. Finally, the results of the measurements are compared to frequency domain results in chapter 7.

Chapter 2

Electromagnetic scattering and Radar Cross Section

This chapter is a short introduction into Radar Cross Section theory, scattering regimes and some high frequency scattering mechanisms. The theory described in this chapter will be used to physically interpret the results of the time domain measurements. A more detailed description of this subject is given by Knott [4].

2.1 Radar Cross Section definition

The Radar Cross Section (RCS) of an object is a measure of its electromagnetic area and is defined as the amount of power that is returned or scattered in a given direction, normalised with respect to the power density of the incident field. The RCS of an object is defined in the far field and is independent of the distance between the radar and the object. Formally, the RCS of an object is defined as [4]

$$\sigma = 4\pi \lim_{R\to\infty} R^2 \frac{|\vec{E}^s|^2}{|\vec{E}^i|^2}$$

where $\vec{E}^i$ and $\vec{E}^s$ represent the incident and scattered field at a range R from the object and σ represents the RCS.

The RCS is a typical frequency domain quantity and is a function of

- frequency,
- object configuration,
- transmitter and receiver polarisation and the
- angular orientation of the object with respect to the incident field.

2.2 Scattering regimes

The ratio between the wavelength of the incident field and the size of the object under test determines the scattering regime of an object. Three regimes are distinguished: low frequency scattering, resonant scattering and high frequency scattering.

2.2.1 Low frequency scattering

If the wavelength of the incident field is much larger than the largest object dimension then the object will behave like a point scatterer. We can assume that there are only little amplitude and phase variations of the incident field over the complete area of the object. The field can be considered as a quasi-static field which builds up opposite charges at the ends of the body. These charges induce a dipole moment which strength is related to the size, the material and the dimension with respect to polarisation of the object.

2.2.2 Resonant scattering

When the wavelength is on the order of the object size the phase variations across the body are much stronger. Every part of the scatterer affects every other part. The scattered field at any point on the body is determined by the sum of the incident field and the scattered field from every other point on the body.

2.2.3 High frequency scattering

When the wavelength is small compared to the largest object dimension, the overall geometry of the object is no longer important. The object is now represented as several independent scattering sources. The total scattered field is determined by the superposition of all these scattering sources.

In the high frequency regime, three scattering mechanisms are distinguished:

- **Specular reflection**

  Specular reflection is limited to a small angular area but in this area the amplitude of the backscattered field is very large. According to Physical Optics (PO) the RCS of a flat plate due to reflection is

  $$\sigma = \frac{4\pi A^2}{\lambda^2}$$

  where σ is the RCS, A is the area of the plate and λ is the wavelength of the incident field.

- **Single diffraction**

  Diffraction is the scattering of electromagnetic fields at the edges, tips or other discontinuities of surfaces. The RCS of a flat plate well away from the specular direction is largely determined by the diffracted waves from its edges.

- **Multiple diffraction**

  Edges does not only diffract the electromagnetic field back to the observer but can also diffract the field in the direction of another edge. The amount of energy scattered by the second edge in the direction of the observer is the double diffraction contribution. Similar to double diffraction, triply diffracted waves are generated (see figure 2.1).

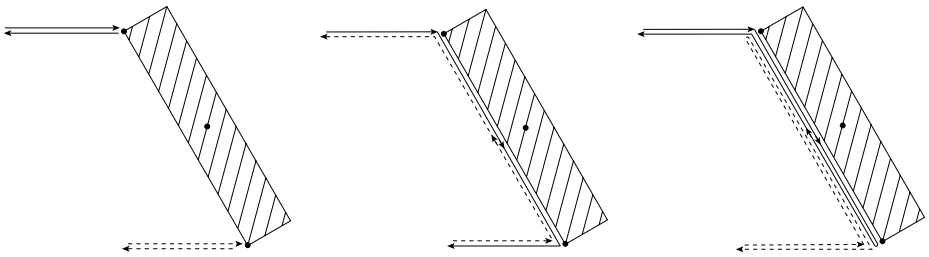

Figure 2.1: Illustration of single, double and triple diffraction mechanism.

Chapter 3

Advantages and limitations of RCS measurements in the time domain

Time domain measurements have several operational and performance related advantages over conventional frequency domain measurements. However, measuring in the time domain also got a limitation.

3.1 Advantages of measuring in the time domain

- **Direct gating**.

  Several unwanted contributions, for example scattering from the surrounding walls or reflections at the transitions (e.g. connectors) in the RF lines, can contribute to the measured field significantly. Direct gating, or windowing in the time domain, utilises the fact that most of these disturbances are separated in time from the backscatter contributions. This property allow us to simply cut the unwanted contributions as long as they do not coincide with the object response.

  Of course one should always try to minimise these unwanted contributions, even if they can be removed later. Because the result of all changes can be observed in real-time it will cost only a small amount of time to find the source of the disturbances and any additional absorbers can be placed directly.

  When the unwanted contributions and the object response do coincide, a small change in length of the cables or position of the object can introduce sufficient time delay to distinguish between the two components.

  For frequency domain measurements this gating would require an additional Fourier transform and the result of the changes in the measurement setup can not be observed real-time.

- **High range resolution**.

  Instead of transmitting a single frequency waveform, an ultra short pulse is fed into the transmitting antenna. The large instantaneous bandwidth provides a very high range resolution without any additional processing.

- **Simple object diagnostics**.

  The positions of scattering sources on the object are easily identified because they are separated in time. This allows directed examination or modification of the object. Again, the result of the modification can be observed real-time.

- **Reduction of measurement time**.

  Time domain RCS measurements can reduce measuring time significantly, thereby reducing the use of scarce measurement facilities. First because the preparation of the measurement setup is faster (see above) and second because the actual measurement is performed faster.

- **Simple measurement setup**.

  Time domain measurements are performed using a relative simple measurement setup.

3.2 Limitations of measuring in the time domain

- **Limited signal to noise ratio**.

  The signal to noise ratio of the received waveform is relatively low compared to frequency domain measurements because the amount of energy contained in the ultra-short pulse is limited. The amount of energy could be increased but, with the current technology, this would inevitably increase the pulse width or decrease the pulse repetition rate.

Chapter 4

Error sources in time domain RCS measurements

4.1 Jitter, thermal and quantisation noise

Noise is electromagnetic energy that limits the detection capabilities of the receiver. Jitter, thermal and quantisation noise will be described quantitatively.

- **Jitter**

  Jitter is the short term variation of the sampling moment. According to the sampling oscilloscope specifications the jitter is less than 2.0 ps. It is assumed Gaussian distributed with zero mean and standard deviation σ_{jitter}. When the local slope of the measured waveform is θ then the amplitude distribution is [1]

  $$\sigma = \sigma_{jitter} \cdot \tan\theta$$

  Assuming that the slope of the measured waveform is constant within the jitter interval the effect of jitter can be reduced by averaging M measured traces.

- **Thermal noise**

  Thermal noise is introduced by the measurement equipment and is very well documented in literature (e.g. [5]). It is assumed to have zero mean and variation $\sigma^2_{thermal}$.

- **Quantisation noise**

  The measured waveform is quantified in discrete levels by the Analog to Digital Converter (ADC). The number of bits of the ADC determines the maximum quantisation error. The error is uniformly distributed over the quantisation interval. Its variation is [1]

  $$\sigma^2_{quantisation} = \frac{q^2}{12}$$

  where $q = 2^n$, the step size of the ADC and n is the number of bits of the ADC.

The combined jitter, thermal and quantisation noise variation is

$$\sigma^2_{combined} = \frac{\sigma^2_{thermal}}{M} + \frac{\sigma^2_{jitter}\tan^2\theta}{M} + \frac{q^2}{12}$$

where M is the number of averaging.

4.2 Time scale inaccuracy

Time scale inaccuracy is the long term accuracy of the sampling time. When for example the sampling time is specified as 20 ps but the real sampling time is 1% longer (20.2 ps) the difference after 2000 samples is 0.4 ns.

4.3 Antenna coupling

There is a significant electromagnetic coupling between the transmitting and receiving antenna because they are in close proximity (see figure 4.1). This coupling can be reduced by increasing the distance between the antennas, but this would inevitably increase the bistatic angle. Also an absorber has been positioned between the antennas. However, because this absorber influences the far field pattern of the antennas and because adequate processing could also remove the coupling contribution it was decided to remove the absorber.

4.4 Reflections

Reflections due to mismatches in the RF lines can overlap with the actual scattering response. This error can be avoided by a careful design of the measurement setup. By variation of the length of the cables they can be shifted to a position where they do not overlap with the scattering response. In the frequency domain these mismatches would introduce standing wave ratios across the RF line which are very difficult to remove.

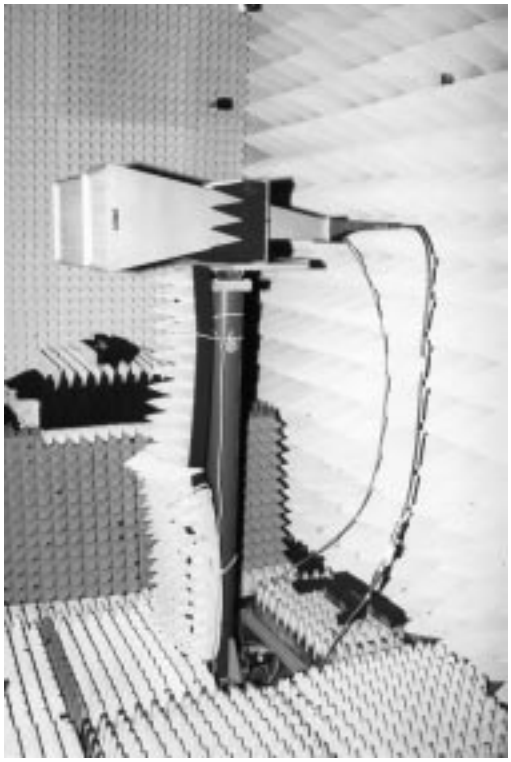

Figure 4.1: Photo of the quasi-monostatic antenna configuration.

4.5 Pulse shape stability

The deconvolution algorithm compares the transmitted and received signal. Because deconvolution is very sensitive to its input signals a small variation can cause much larger variations after deconvolution. This means that the short and long term stability of the pulse generator is very important.

Chapter 5

Description of the time domain RCS measurements

This chapter describes the setup of the RCS measurements, gives a mathematical description of these measurements in time and frequency domain and describes the important parameters of the measurement equipment.

5.1 Measurement setup

As described earlier, only specially designed transient antennas can transmit the ultra-short input pulse at their feed. Because these antennas were not available at IRCTR an alternative approach has been taken. Two ridged horn antennas are used to transmit the pulse. The transmitted electromagnetic field does not have an ultra-short pulse shape, but it does contain all the information to reconstruct the impulse response of the object under test from the received signal. For this approach an additional system transfer measurement is necessary to determine the antenna characteristics.

Summarising, three measurements will be performed to extract the scattering characteristics of the object under test:

1. **A system response measurement**. The system response measurement determines the transfer function or impulse response of the system as described above.

2. **An object measurement**. The object measurement determines the total scattered field.

3. **A background measurement**. The background measurement determines the clutter (empty room scattering contributions and antenna coupling).

All measurements are performed with vertical transmitter and receiver polarisation.

The minimal RCS (σ_{min}) which can be measured is determined via the radar range equation [6]

$$\sigma_{min} = \frac{1}{SNR_{pulse}} \cdot \frac{(4\pi R^2)^2}{G_t G_r} \frac{4\pi}{\lambda^2}$$

The results for 2 and 12 GHz are shown in table 5.1.

The gain of the horns is provided by their datasheet and the signal to noise ratio of the pulse is provided by [2].

	2 GHz	*12 GHz*	
$1/SNR_{pulse}$	-70.0	-50.0	dB
$(4\pi R^2)^2$	41.6	41.6	$dB \cdot m^4$
$1/(G_t G_r)$	-30.0	-52.0	dB
$4\pi/\lambda^2$	27.5	43.0	$dB \cdot m^{-2}$
σ_{min}	-30.9	-17.4	$dB \cdot m^2$

Table 5.1: Minimal detectable RCS (σ_{min}) at 2 and 12 GHz.

5.1.1 System response measurement

The system response measurement determines the impulse response of the measurement system. The response is dominated by the combined antenna response but also contains contributions from the cables (dispersion and attenuation), connectors and pulse generator. The system response measurement removes the need for transient antennas. A deconvolution of the object measurement and the system response reconstructs the impulse response of the object under test. The response is measured using the setup shown in figure 5.1.

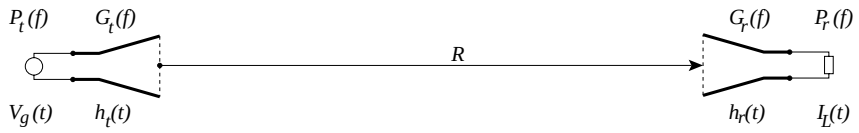

Figure 5.1: Experiment setup of the system response measurement.

The antennas are aligned for maximum directional radiation and reception. An additional 20 dB attenuator has been inserted between the receiving antenna and the sampler to avoid damage by too high input voltages.

The pulse generator is positioned in the pit below the transmitting pedestal. It is triggered via a long trigger cable through the tunnel from the sampling scope. The sampler is outside the anechoic chamber.

To avoid any change in parameters, the system response measurement should be performed using *exactly* the same equipment as the object measurement. Ideally, no connectors should be touched because friction can cause changes. Practically, this is impossible. To minimise changes only one SMA-type connector has been disconnected and the 20 dB attenuator has been inserted.

5.1.2 Object measurement

The total backscattered field from the environment and the object is determined by the object measurement. The two similar antennas are laser aligned and point to the centre of the object. This introduces a bistatic angle of approximately 6 degrees. This angle could be avoided by using a single antenna. However, the additional hardware required to separate the transmit and receive signal with a single antenna would also further decrease the signal to noise ratio. A second reason is that the measurements will be compared to data which is also measured with a small bistatic angle.

The distance between the front plane of the antennas and the object is 3.10 meter ($R_1 = R_2$).

In front of the pedestal some additional absorbing material is positioned to reduce the scattering from the pedestal and the X-Y table (see figure 5.6). The exact position of

the absorber is determined by trial and error. To reduce scattering from the pedestal an additional absorber is mounted around the top.

The pulse generator and the sampler are positioned outside the anechoic chamber. Sucoflex cables are used to connect them to the pulse shaper and antennas. The length of the cable between the pulse generator and the pulse shaper has to be longer than 3 meters (see section 7.1.2).

5.1.3 Background measurement

The background measurement determines the backscatter of the empty room. Assuming the scattering is stationary it can be subtracted from the object measurement to reduce clutter and direct antenna coupling.

The measurement setup for the background measurement is almost identical to the object measurement setup. The only difference is the absence of the object under test. The background measurement is performed just before or after the object measurement for optimal stability.

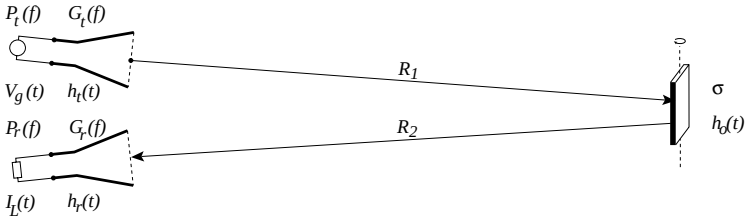

Figure 5.2: Experiment setup of the scattering measurement.

5.2 Frequency domain description of the measurements

In this section a frequency domain description for the measurement system is given. It will be used to show the equivalence between the frequency domain and time domain description.

5.2.1 An expression for the system response measurement

The measurement setup of the calibration measurement is shown in figure 5.1. The calibration measurement is described by the well known Friis Transmission Equation [6]

$$\frac{P_r}{P_t} = \left(\frac{\lambda}{4\pi R}\right)^2 G_t(f) G_r(f)$$

In this equation, P_t and P_r represent the transmitted and received power respectively. λ is the wavelength of the transmitted signal and R is the range (distance) between the two antennas. $G_t(f)$ and $G_r(f)$ are the gains of the transmitting and receiving antenna.

5.2.2 An expression for the object measurement

The relation between the transmitted and received power in figure 5.2 is described by the radar range equation [5]

$$\frac{P_r}{P_t} = \sigma \frac{G_t(f) G_r(f)}{4\pi} \left[\frac{\lambda}{4\pi R_1 R_2}\right]^2$$

or

$$\sigma = \frac{P_r}{P_t} \frac{4\pi}{G_t(f)G_r(f)} \left[\frac{4\pi R_1 R_2}{\lambda}\right]^2$$

where σ is the RCS of the object under test. P_r and P_t are known and the system response measurement provides the combined antenna gain $G_t(f)G_r(f)$.

5.3 Time domain description of the measurements

Now we have seen the frequency domain expressions for the experiment, an equivalent time domain expression is derived. The expressions are based on Shlivinski's time domain antenna characterisation [7] and use the load current instead of the power to characterise the system. Power P and load current I_L are related by

$$P = I_L^2 Z_0$$

where Z_0 is the characteristic impedance of the system.

5.3.1 Time domain system response measurement

According to Shlivinski the resistor load current $I_L(t)$ for a setup using two identical antennas (figure 5.1) is

$$I_L(t) = \frac{1}{4\pi R} \frac{c^{-1}\eta}{2Z_{0T}Z_{0R}} \left[(\mathbf{h}_t(\mathbf{r}_{TR}, \cdot) * \mathbf{h}_r(\mathbf{r}_{RT}, \cdot)) * V_g(\cdot)\right](\tau - t_g - t_L)$$

where $\eta = \sqrt{\frac{\mu}{\epsilon}}$ is the free space wave impedance, $\mathbf{h}_t$ and $\mathbf{h}_r$ are the effective heights of the transmitting and receiving antenna (the effective height is a time domain equivalent of the antenna gain function and can be considered as the impulse response of an antenna) and V_g is the generator voltage waveform. The last term in this expression $(\tau - t_g - t_L)$ is an index of the convolution term between the square braces. The $\cdot$ is an arbitrary variable.

5.3.2 Time domain object measurement

The above expression for I_L is now expanded for the experiment setup of figure 5.2. First the incident electric field at the object is determined. Then a time domain scattering function is defined, which is used to derive an expression for the load current.

The electric field at the object is

$$\mathbf{E}(\mathbf{r}, t) = -\frac{1}{4\pi R_1} \frac{c^{-1}\eta}{2Z_0} \left[V_g(\cdot) * \mathbf{h}_t(\mathbf{r}, \cdot)\right](\tau - t_g)$$

The time domain scattering function $h_o(t)$ is defined as the far-field impulse response of the object. Using this definition the electric field at a distance R_2 of the object is

$$\mathbf{E}(\mathbf{r}, t) = -\frac{1}{4\pi R_1} \frac{1}{4\pi R_2} \frac{c^{-1}\eta}{2Z_0} \left[(V_g(\cdot) * \mathbf{h}_t(\mathbf{r}, \cdot)) * \mathbf{h}_o(\mathbf{r}, \cdot)\right](\tau - t_g)$$

The load current due to this electric field is

$$I_L(t) = -\frac{1}{Z_0} \left[\mathbf{h}_r(\mathbf{r}, \cdot) * \mathbf{E}(\cdot)\right](t - t_L)$$

or

$$I_L(t) = \frac{1}{4\pi R_1}\frac{1}{4\pi R_2}\frac{c^{-1}\eta}{2Z_{0T}Z_{0R}}\left[((\mathbf{h}_t(\mathbf{r}_{TR},\cdot) * \mathbf{h}_r(\mathbf{r}_{RT},\cdot)) * \mathbf{h}_o(\mathbf{r},\cdot)) * V_g(\cdot)\right](\tau - t_g - t_L)$$

The (combined) antenna impulse response $h_a(t) = V_g(\cdot) * (\mathbf{h}_r(\mathbf{r}_{RT},\cdot) * \mathbf{h}_t(\mathbf{r}_{TR},\cdot))\,(\tau - t_g - t_L)$ is determined from the system response measurement.

The object impulse response $h_o(t)$ is obtained by performing a deconvolution of the measured object response and the system response.

5.4 Description of the measurement equipment

The Russian time domain measurement system K2-63 is used for the measurements. It consists of a sampling oscilloscope (including a sample unit) and a pulse generator.

5.4.1 Sampling oscilloscope

The K2-63-1 sampling oscilloscope (see figure 5.3) is the centre of the measurement system. It provides the pulse generator and sample unit with trigger pulses and collects and displays the measured data. The sampling unit K2-63-3 is a subsystem of the sampling scope. The bandwidth of the input channel is 0–18 GHz. To avoid time scale inaccuracy the time scale is calibrated with the internal reference signal (derived from a crystal oscillator) before every measurement. The data from the sampling scope is transferred to a Pentium PC and stored.

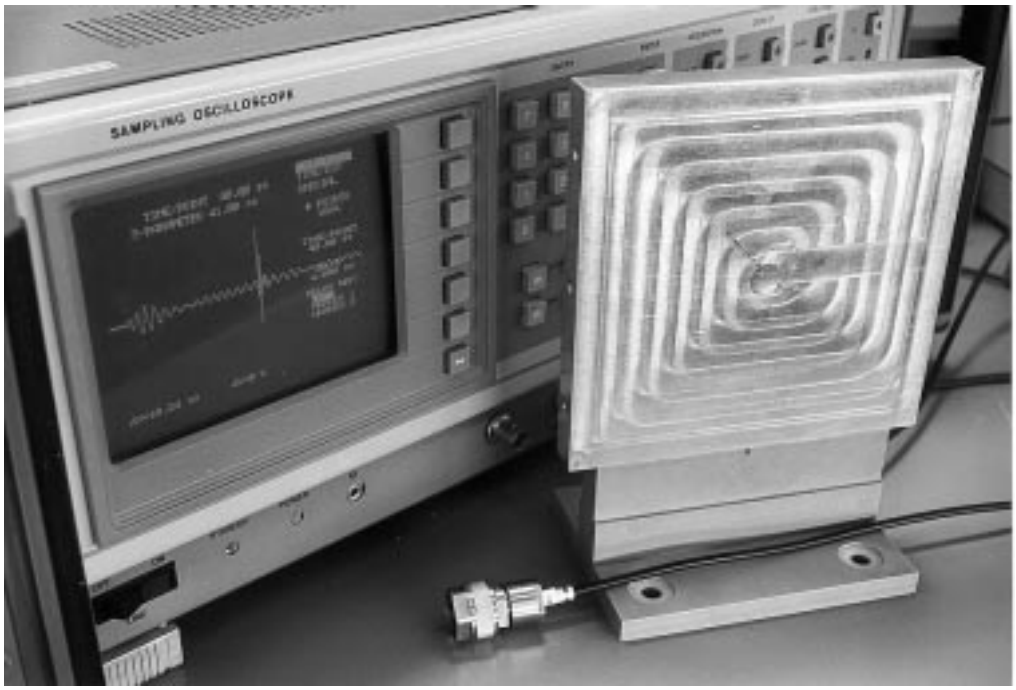

Figure 5.3: Photo of the sampling scope and the object under test.

5.4.2 Pulse generator

The pulse generator (K2-63-2) with external pulse shaper 1 produces pulses with an 50% amplitude width of 85 ps, a peak voltage of 30 V at a pulse repetition rate of 100 kHz. Figure 5.4 shows the pulse voltage at the pulse shaper output. The original 30 V amplitude has been attenuated by the long cables and by a 40 dB attenuator which is inserted to avoid too high input voltages at the sampler input. The pulse generator is triggered from the sampling scope.

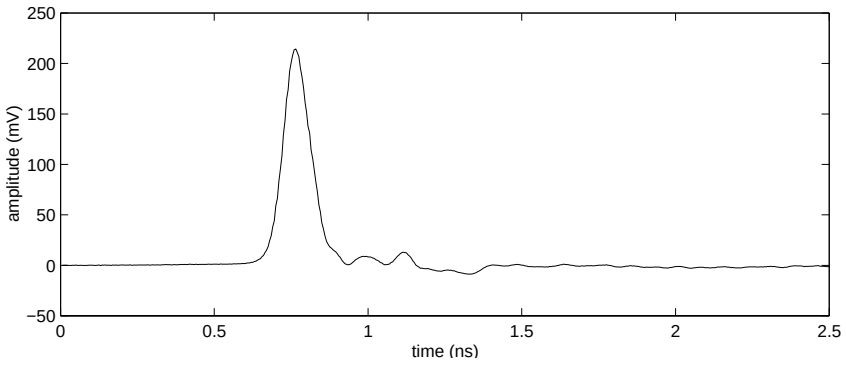

Figure 5.4: Time domain signal at the pulse shaper output.

5.4.3 Cables

For all measurements Sucoflex cables are used. During the preparation it was shown that the connections between the cables and the devices need special attention. When the connectors are not tightened very carefully they can introduce severe distortion. The distortion ranges from small deviations of the waveform to the generation of additional RF line reflections. Figure 5.5 shows the result of an object measurement using an alternative cable (compare to figure 7.3(b)). The distortions in the negative peak are caused by bad connectors.

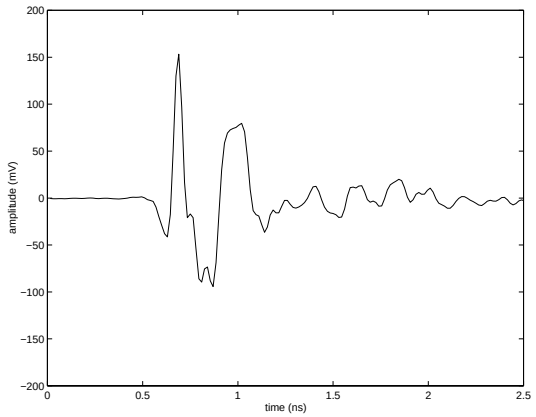

Figure 5.5: Measured object response using cables with bad connectors.

5.4.4 Environment, the Delft University Chamber for Antenna Tests (DUCAT)

The Delft University Chamber for Antenna Tests is a shielded environment (shielding at least 120 dB) of 3 x 3 x 6 meters. The inside of the chamber is covered with absorbing material to reduce scattering from the walls. The antennas and the object under test are mounted on two pedestals with a mutual distance of 3.5 m. The distance between the object and the back wall is 77 cm. The time delay between the object and back wall scattering is $\frac{2 \cdot 0.77}{3 \cdot 10^8} = 5.1$ ns. This is long enough to prevent overlap of both signals.

5.4.5 Antennas

The antennas are a critical component of the measurement system. Their bandwidth is limiting the bandwidth of the complete measurement system. To properly transmit and receive ultra short pulses both antennas should have a large bandwidth. For most wideband horn antennas the phase centre moves as a function of frequency. Therefore it is impossible to preserve the ultra short pulse shape unless special transient antennas are used.

An additional effect is the ringing of the transmit antenna. The ultra short input pulse excites several resonant frequencies. These frequencies are still transmitted when there is no signal at the input terminal of the antenna which introduce a significant tail.

Two identical Russian ridged horn antennas (2–12 GHz) are used to transmit and receive the short pulses. Their gain is specified from 15 dB at 2 GHz to 27 dB at 12 GHz.

The antennas are mounted on the pedestal using two specially made aluminium adapters (see figure 4.1).

5.4.6 Object

The object under test is an aluminium plate with one flat side (see figure 5.3) and one artificial rough side (see figure 5.6). The size of the plate is 148 x 148 x 15.7 mm. Detailed information concerning the plate and the scattering from this plate (calculations and measurements) is provided by Pieper [8]. The plate is selected because

- it is well documented,
- it has a relative large RCS and
- the plate itself and its mount are already available.

The object is mounted on a pedestal which can rotate around the azimuth axis and translate in the X-Y surface. The X-Y table is fixed at the reference position $(0, 0)$.

Figure 5.6: Photo of the object pedestal.

Chapter 6

Functions and implementation of the signal processing

The software processing of the measured data has three purposes:

1. signal to noise ratio improvement,
2. clutter suppression and
3. resolution enhancement.

Most of the processing techniques are adopted from geophysical science.

6.1 Signal to noise ratio improvement

The sampling oscilloscope has a built-in averaging function which measures M traces and determines the average amplitude at each instant. For all the measurements described in this report $M = 256$. The integration gain achieved is $10 * \log M = 24.2$ dB.

6.2 Clutter suppression

Clutter is defined as the scattering contributions which do not originate from the object under test. For example reflections from the walls of DUCAT or backscatter from the pedestal are classified as clutter. Also the direct coupling from the transmitting to the receiving antenna is considered as clutter because it can be removed with the same processing techniques. Interactions between the object and the environment (for example when the scattered field is reflected via the walls to the receiving antenna) will be very small and are ignored.

6.2.1 Subtraction

Assuming that clutter is stationary, it can be removed by subtraction of the empty room response from the object response. Care must be taken not to change any sampling scope parameters (i.e. sample time or delay settings) because the time scale of the object and background response must fit exactly. The background measurement has to be performed directly before or after the object measurement to avoid drift.

The subtraction of the background from the object introduces an additional error: during the object measurement, part of the back wall is in the shadow region of the object, so there will be no scattering contribution from this part of the wall. However, during the background measurement the object is removed and the region directly behind the object is illuminated by the antenna. When the background is subtracted from the object measurement, we are actually subtracting too much. This contribution is expected $\frac{2 \cdot 0.77}{3 \cdot 10^8} = 5.1$ ns after the arrival of the plate response and can be observed in figure 7.3(a). This error will have no further consequences because it is easily gated out. It can be avoided by placing absorbers in front of the object instead of completely removing the object during the background measurement.

6.2.2 Gating

The second method to remove clutter from the measurement is gating or time domain windowing. Every clutter contribution which does not overlap with the object response is ignored.

6.3 Resolution enhancement

The incident field at the object is not an infinite short pulse and thus the measured response will not be an impulse response. However, the received waveform contains sufficient information to reconstruct the impulse response. This reconstruction, or pulse compression, is performed with a software deconvolution algorithm.

The deconvolution is implemented with a least squares based algorithm [9]. According to Hayward [10] this method gives good results even for relative low signal to noise ratios. The algorithm determines the pseudoinverse of the antenna response with a singular value decomposition. Each singular value corresponds to a small range of frequencies [11]. According to Rahman [12], satisfactory results are obtained when the number of singular values is proportional to the (estimated) signal to noise ratio of the input signal. Every singular value which is smaller than the value of the largest singular value divided by the signal to noise ratio is ignored.

A bandpass filter is applied to the deconvolved result to remove all contributions which are outside the antenna bandwidth. It is important to conserve the phase relation between the frequency components because otherwise the time domain signal would be heavily distorted. An eight order linear phase bandpass filter is implemented in MATLAB. Its frequency domain transfer function is shown in figure 6.1.

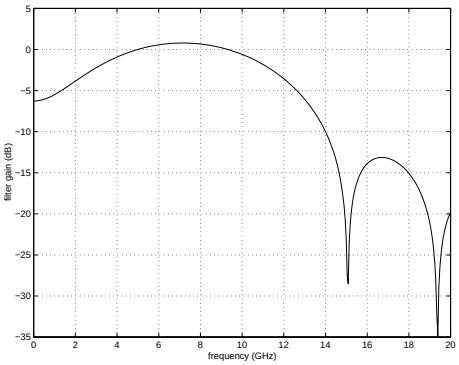

Figure 6.1: Transfer function of the linear phase bandpass filter.

Chapter 7

Interpretation and discussion of the results

This chapter contains the results of the time domain RCS measurements before and after processing, a physical interpretation and a comparison with predicted and measured frequency domain results.

7.1 Time domain results

The time between two samples (sample time) for all time domain measurements is 20 ps. The delay is adjusted for each measurement.

7.1.1 System transfer measurement

The result of the system transfer measurement is shown in figure 7.1(a).
Two regions can be identified in the system response:

1. **The early time region**

   This is the region in which the antenna is fed with an input signal and transmits a derivative of this signal. The area is characterised by its relatively wide frequency spectrum.

2. **The late time region**

   The input signal of the antenna excites oscillations at several frequencies which continue ringing when the feed signal has stopped. The power spectrum of the late time region only contains energy at (relatively low) resonant frequencies. The dominant frequency is 900 MHz, which is the lower cut-off frequency of the antennas.

The power spectrum of the complete system impulse response is shown in figure 7.1(b).

7.1.2 Object measurement

The result of the broadside object measurement is shown in figure 7.2(a). The relative low frequency component is coupling between the transmit and receive antenna. The large response after 22 ns is the backscatter of the object. The signal between 30 and 35 ns is caused by reflections in the RF line, probably at the antenna input and the pulse shaper

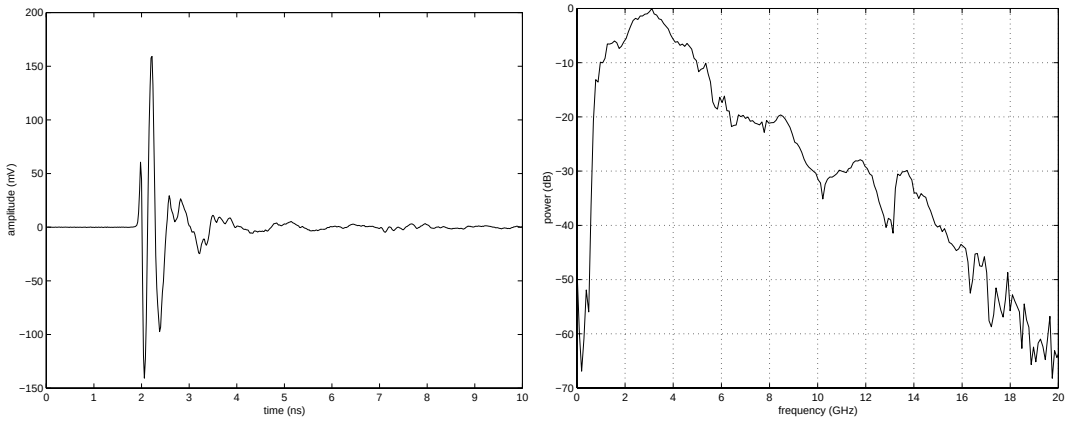

(a) (b)

Figure 7.1: Measured system impulse response (a) time domain waveform, (b) calculated power spectrum.

output (the reflection is *not* caused by the pulse shaper input because this reflection is much larger and positioned 30 ns after the object response). This reflection is also transmitted and scattered by the object.

The very small signal at 18 ns is caused by backscatter from the absorbers in front of the pedestal, see figure 5.6 (the absorbers are approximately 60 cm or $\frac{2 \cdot 0.60}{3 \cdot 10^8} = 4$ ns before the object response). This has been verified by moving the absorbers in the direction of the antennas. The backscattered signal was indeed shifted forward according to the distance of the movement.

7.1.3 Background measurement

The result of the background measurement in shown in figure 7.2(b). As expected the direct coupling between the antennas has not changed. Also the backscatter from the absorbers is still observed.

7.1.4 Result after background subtraction

Figure 7.3(a) shows the complete time window of the measured object response with the background subtracted. The signal between 20 and 25 ns is the scattered signal from the flat plate. Figure 7.3(b) shows a close-up of this signal. The error caused by subtraction of too much background (see section 6.2.1) is observed between 25 and 30 ns.

7.1.5 Result after deconvolution

The result of the deconvolution of the signals in figure 7.3(b) and 7.1(a) is shown in figure 7.4(a). The deconvolved signal after bandpass filtering is shown in figure 7.4(b).

The processed scattering response for rotation angles of the object between 10 and 50 degrees is shown in figure 7.5. The physical interpretation of these waveforms is explained

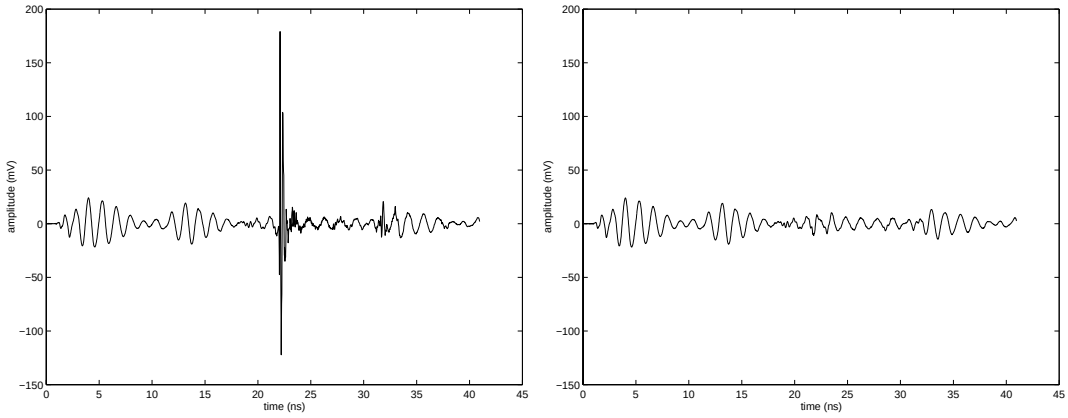

(a) (b)

Figure 7.2: Time domain results of (a) the object measurement, (b) the background measurement.

below. To verify my interpretation I also requested L.J. van Ewijk (TNO-FEL) for an interpretation. His interpretation corresponds to the interpretation described below.

- **Specular reflection**

  The backscattered signal in figure 7.4(b) is almost only due to specular reflection. The shape of the reflected waveform is explained by the frequency dependence of the scattered power of the flat plate. This dependence translates to a differentiation in the time domain. This is verified by a comparison of the object response (figure 7.3(b)) and the numerically differentiated, scaled and shifted antenna response, see figure 7.6.

- **Single diffraction**

  When the flat plate is rotated the reflection contribution decreases rapidly. The edge diffraction of the incident field increases and becomes dominant.

  At 10 degrees rotation the first negative (and largest) peak is interpreted as the backscatter from the leading edge of the flat plate (edge 1 in figure 7.7). The largest positive peak is the backscatter from the trailing edge.

  The time delay between the leading and trailing edge is related to the difference in propagation path length. The delay increases for increasing rotation angles. From figure 7.7 we can evaluate the time delay for all rotation angles. The short dotted lines in figure 7.5 represent the predicted positions of the edge diffractions. The 20 degrees measurement is used as the reference for these calculations. See also figure 7.8. The positions of the calculated and measured peaks correspond exactly (i.e. up to 20 ps).

  From these comparisons it is concluded that the time scale of the sampling scope is stable and that no significant time scale inaccuracy can be measured.

- **Multiple diffraction**

  The multiple diffractions can be identified by examining their propagation path lengths. The doubly diffracted field has a constant delay compared to a reference plane in front

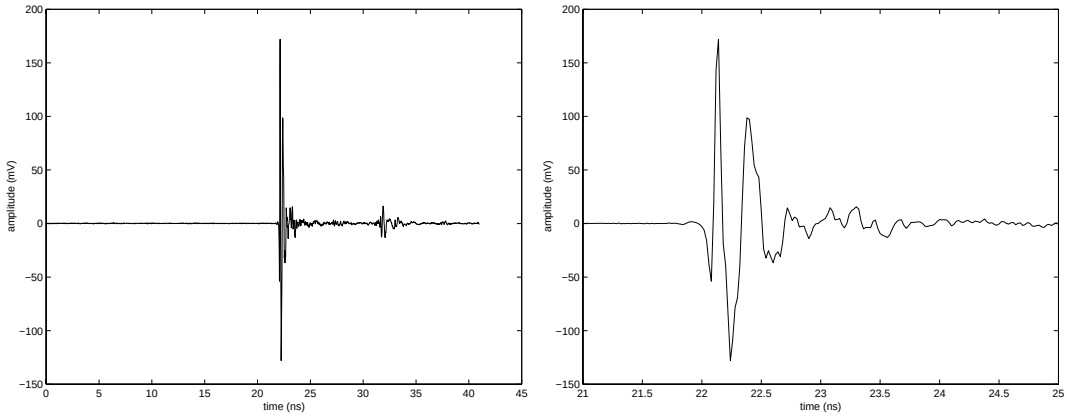

(a) (b)

Figure 7.3: Time domain object response after background subtraction (a) complete time window, (b) gated response

of the plate for all rotation angles. The triply diffracted field has a constant delay compared to the leading edge. In figure 7.5 the doubly diffracted field is marked by the long vertical dotted line. The triply diffracted field is marked by the dots on top of the waveform.

As shown in figure 2.1 two propagation paths for each doubly and triply diffracted field exists. These two contributions are equal (reciprocity).

From these measurements the group-velocity of the surface wave can be determined. The measured velocity is approximately $1.8 \cdot 10^8$ m/s, 60% of the travelling wave velocity in vacuum.

The opinions concerning this velocity differed along several people:

1. The measured velocity is *correct*. The surface wave is slowed down significantly by the conducting surface. Also the thin layer of aluminium oxide at the top of the surface will slow down the wave. This would support the multiple diffraction interpretation.
2. The measured velocity is *incorrect*. Because the surface wave is travelling through free space its speed will be approximately $c = 3.0 \cdot 10^8$ or at least a few percent slower. This implies that the given interpretation of the results (separation between multiple diffractions) is incorrect.

Additional experiments using a different object can give more details about the measured velocity. Does it change for changing plate dimensions? What happens when a gold or silver plated object is used instead?

7.2 Frequency domain results

The frequency domain RCS is obtained from the time domain measurements via a Fourier transform. The gated object response is 300 points long, resulting in a frequency resolution

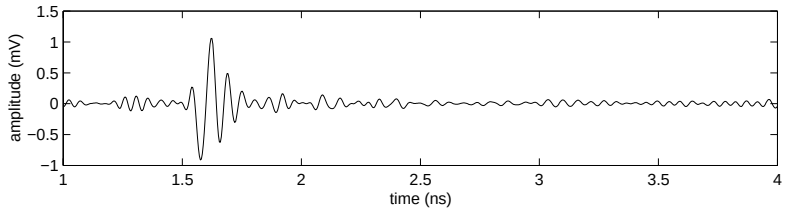

(a)

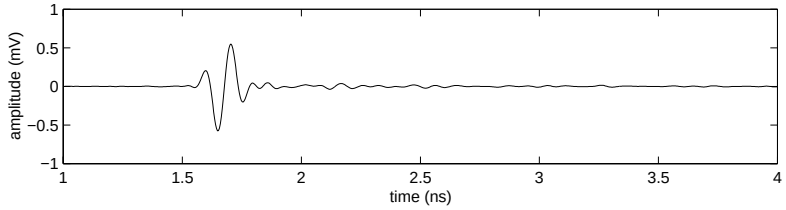

(b)

Figure 7.4: Result of the deconvolution performed on the signals of figure 7.3(b) and 7.1(a). (a) before filtering, (b) after bandpass filtering.

of $\frac{50 \cdot 10^9}{299} = 0.17$ GHz.

7.2.1 Comparison of the measured and predicted RCS

The RCS of an identical sized flat plate without the roughness is calculated with the TNO-FEL RCS prediction software RAPPORT (Radar signature Analysis and Prediction by Physical Optics and Ray Tracing). RAPPORT is a high frequency code and predicts the physical optics contribution of the RCS of an object. The results of RAPPORT and the transformed time domain measurements are compared at three frequencies along the antenna bandwidth: 2.2, 8 and 12 GHz. The results are shown in figure 7.9. The measured RCS is normalised to correspond exactly at 0 degrees because no additional calibration measurement has been performed.

The calculated nulls are much deeper than the measured nulls because the calculations does not include any diffraction contribution. In the measured results these diffraction contributions has 'filled' the deep nulls.

At 2.2 GHz there is a good agreement for angles up to 20 degrees. Note that this prediction is not realistic because it uses a high frequency estimation of the scattering contributions. At 2.2 GHz the size of the plate is only $1.1\lambda \times 1.1\lambda$. For aspect angles above 40 degrees the measured RCS is larger than the calculated. A possible explanation for this is the rough backside of the plate. Especially at low frequencies there will be backscatter from the backside, even when it is not optically visible.

As expected there is a better correspondence of the positions and widths of the mainlobe and its sidelobes at 8 GHz. The high RCS level at 90 degrees is caused by backscatter

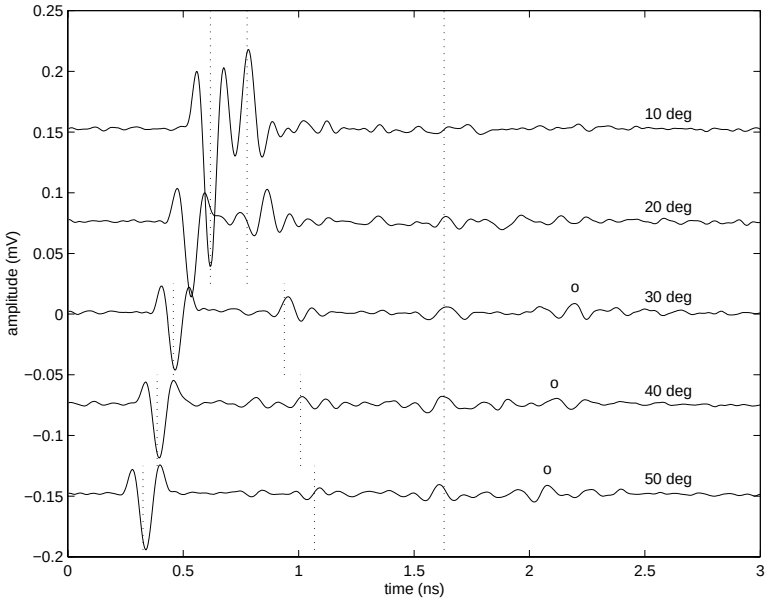

Figure 7.5: Processed flat plate response for rotation angles from 10 to 50 degrees

from the side area of the plate. The absence of diffraction contributions in the RAPPORT calculation could explain the differences between the predicted and measured RCS for angles of incidence larger than 40 degrees.

At 12 GHz there is still a good correspondence of the positions and widths of the mainlobe and its sidelobes. As expected the signal to noise ratio has decreased. According to table 5.1 the noise floor (or minimal detectable RCS) is approximately at -17.4 dB $\cdot$ m^2. For angles of incidence above 80 degrees the rough backside of the plate becomes optically visible, resulting in a higher RCS than predicted.

Figure 7.10 shows the measured and calculated frequency dependance of the broadside RCS. Because the deconvolution determines the relation between the frequency components by elimination of the antenna transfer function this plot is an indication of the deconvolution performance.

From this figure the agreement between measurement and prediction is good between the specified antenna limits (2–12 GHz). The maximum error is 2 dB.

7.2.2 Comparison of time and frequency domain measurements

The transformed time domain data is also compared to frequency domain measurements from Pieper [8]. These measurements are also performed in DUCAT using exactly the same object and mounting structure. The results are shown in figure 7.11. The transformed time domain data is normalised because no calibration measurement is performed.

The signal to noise ratio of the time domain measurements seems less than the frequency domain SNR. However, additional examination of the measurement system should show whether these effects are really caused by the limited signal to noise ratio.

From these comparisons we can conclude that the time domain equipment can be used to perform RCS measurements. The purpose of each experiment determines whether time or frequency domain measurements are favourable.

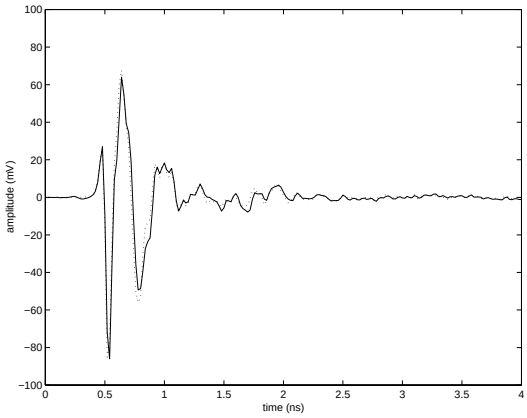

Figure 7.6: Comparison of the object response (dotted) and the numerically differentiated, amplitude scaled and shifted antenna response (solid).

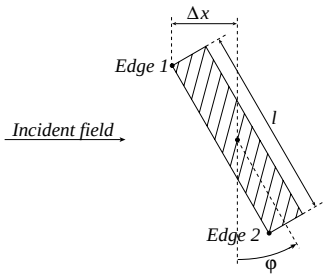

Figure 7.7: Distance Δx as function of azimuth angle φ

7.3 Comparison with time domain measurements from literature

The resolution of the measurements after processing is approximately 100 ps. This is very high compared to recent literature. Only Morgan [13] reports similar results. He describes the single diffraction contributions from a thin wire but does not describe the multiple diffraction contribution.

Several other articles mention the separation of leading and trailing edges, for example Madonna [14], but these observations are very doubtful because of the very limited range resolution (1 ns or worse).

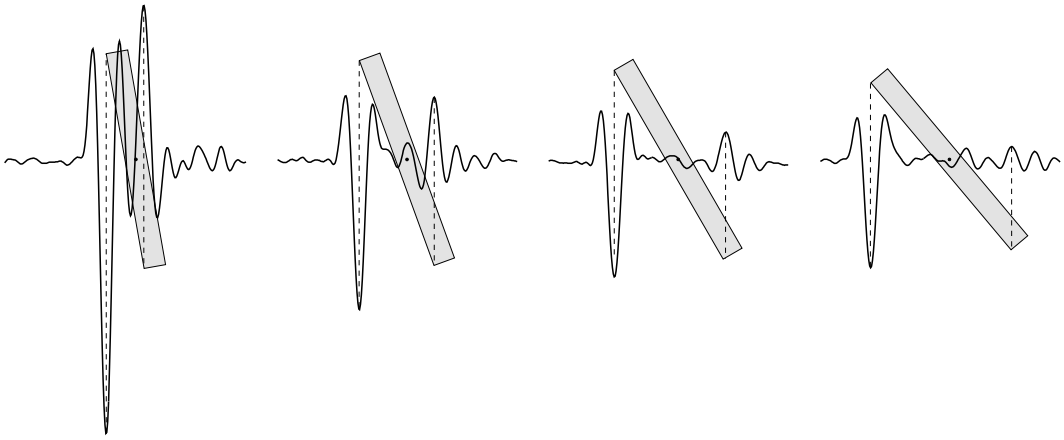

Figure 7.8: Calculated and measured positions of leading and trailing edge diffractions.

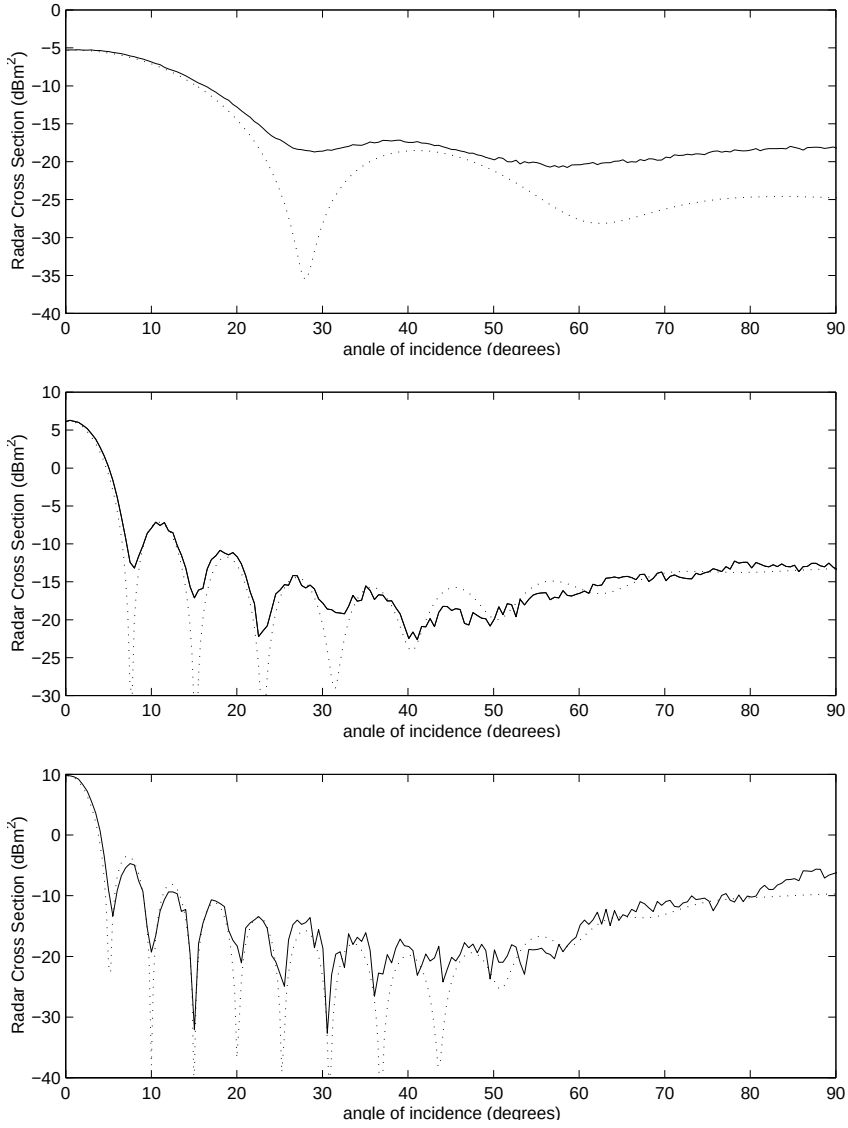

Figure 7.9: Predicted (dotted) and measured (solid) RCS of the flat plate. Upper plot 2.2 GHz, Middle plot 8 GHz, Lower plot 12 GHz.

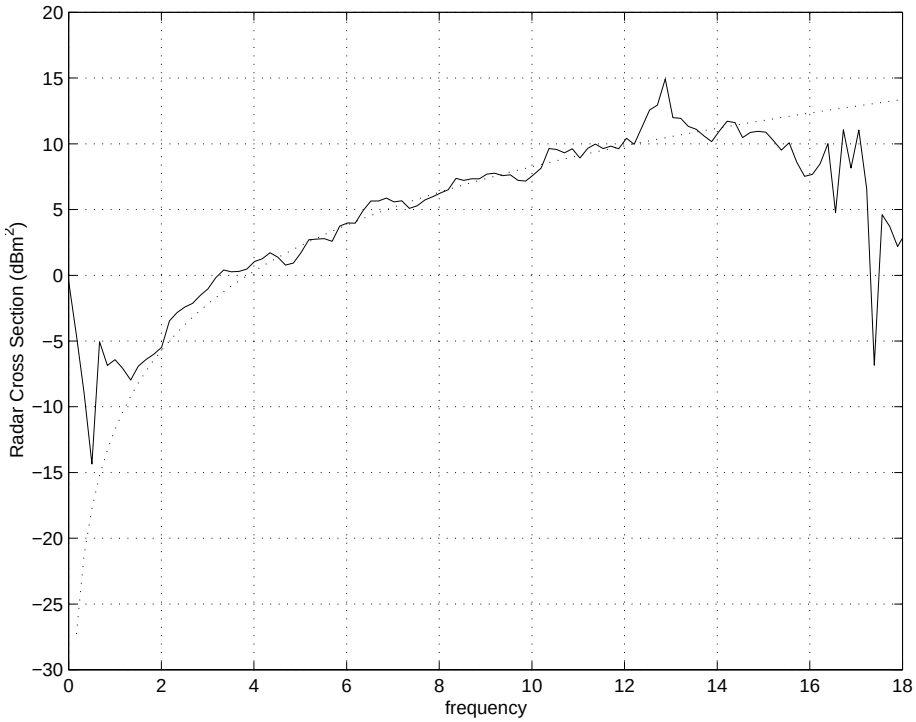

Figure 7.10: Measured and calculated frequency dependence of the broadside RCS of a flat plate. The measured RCS is normalised to the calculated RCS for one frequency.

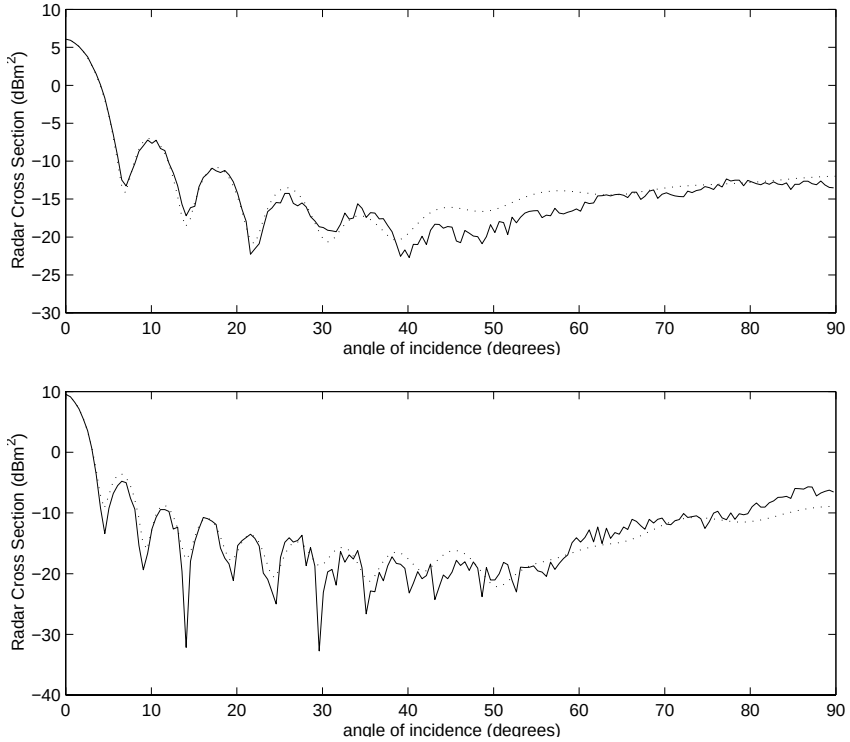

Figure 7.11: Comparison of transformed time domain measurements (solid) and frequency domain measurements (dotted) of the flat plate. Upper plot 8 GHz and lower plot 12 GHz.

Chapter 8

Conclusions and recommendations

8.1 RCS measurement conclusions

- **The time domain equipment can be used for high resolution Radar Cross Section measurements.**

  The results are compared to calculated and measured frequency domain results and show a good agreement.

- **The usage of non transient-optimised antennas in combination with software processing gives good results.**

  The high resolution (better than 100 ps) of the time domain results enables separation of scattering mechanisms (i.e. reflection, single and multiple diffraction). This resolution is not provided by special transient antennas but by the application of a software range compression algorithm.

- **The signal to noise ratio of the measurements agrees with the SNR expected from the radar range equation.**

  The signal to noise ratio decreases for increasing frequencies and is sufficient to determine the scattering characteristics of the flat plate. As expected, the SNR is lower compared to frequency domain measurements.

- **The normalised Fourier transformed time domain measurements show a good agreement with frequency domain measurements**.

As a final conclusion it can be stated that time domain RCS measurements are an attractive alternative of its frequency domain equivalent. However, the decision to measure in time or frequency will depend on the specific aim of each experiment.

8.2 Recommendations for future RCS measurements

- A closer examination of the measurement system has to reveal the system performance. Several differences between frequency and time domain measurements can not be explained and are not likely to be caused by the limited signal to noise ratio (e.g.

what is the effect of the bistatic angle on the deconvolution performance because the system response was measured without a bistatic angle?).

- Instead of the system response measurement also a measurement of a (well known) reference object could provide the antenna response. This would avoid changing the measurement setup, which could be difficult in operational environments.
- Absolute RCS measurements can be performed by calibration of the measurement system with an exactly known object. This measurement provides a calibration curve which can be used to calibrate the object measurement.
- Finally, the multiple diffraction interpretation can be verified or rejected by measuring
  - multiple polarisations,
  - plates of different sizes,
  - gold or silver plates and
  - a very thin plate.

Bibliography

[1] Rene V. de Jongh. The fundamentals of time domain antenna measurement. Technical Report IRCTR-S-001.96, International Research Centre for Telecommunication -transmission and Radar, July 1996.

[2] Rene V. de Jongh. Time domain antenna measurement report. Technical Report IRCTR-S-002.96, International Research Centre for Telecommunication -transmission and Radar, July 1996.

[3] Rene V. de Jongh, M. Hajian, and L.P. Ligthart. Antenna time-domain measurement techniques. *IEEE Antennas and Propagation Magazine*, October 1997.

[4] Eugene F. Knott, John F. Shaeffer, and Michael T. Tuley. *Radar Cross Section, its Prediction, Measurement and Reduction.* Artech House, 1985.

[5] Merrill I. Skolnik. *Introduction to Radar Systems.* McGraw-Hill, 1980.

[6] Constantine A. Balanis. *Antenna Theory, Analysis and Design.* John Wiley & Sons, 1982.

[7] Amir Shlivinski, Ehud Heyman, and Raphael Kastner. Antenna characterization in the time domain. *IEEE Transactions on Antennas and Propagation*, July 1997.

[8] Wouter J.C. Pieper. Scattering from an artificial rough surface, calculation and measurement. Master's thesis, Delft University of Technology, December 1995.

[9] Edward J. Rothwell and Weimin Sun. Time domain deconvolution of transient radar data. *IEEE Transactions on Antennas and Propagation*, April 1990.

[10] G. Hayward and J.E. Lewis. Comparison of some non-adaptive deconvolution techniques for resolution enhancement of ultrasonic data. *Ultrasonics*, May 1988.

[11] M.P. Ekstrom. A spectral characterization of the ill-conditioning in numerical deconvolution. *IEEE Transactions on Audio and Electroacoustics*, August 1973.

[12] Jahangir Rahman and Tapan Kumar Sarkar. Deconvolution and total least squares in finding the impulse response of an electromagnetic system from measured data. *IEEE Transactions on Antennas and Propagation*, April 1995.

[13] Michael A. Morgan. Ultra-wideband impulse scattering measurements. *IEEE Transactions on Antennas ans Propagation*, June 1994.

[14] R.G. Madonna, P.J. Scheno, and J. Scannapieco. Diffraction of ultrawide band radar pulses. In *SPIE Proceedings on Ultrawideband Radar*, 1992.

[15] David Daniels. Applications of impulse radar technology. In *Radar 97*, October 1997.

[16] M.N.R. Remijn. Antenna and radar cross section measurement in the Delft anechoic chamber. Master's thesis, Delft University of Technology, June 1990.

[17] Wim. A. van Cappellen. Evaluation of multiple diffraction coefficients using the uniform theory of diffraction. Technical Report FEL-97-S061, TNO Physics and Electronics Laboratory, February 1997.

[18] Shane Cloude, Paul Smith, and Alec Milne. Analysis of time domain ultra wideband radar signals. In *SPIE Proceedings on Ultrawideband Radar*, 1992.

Appendix A

MATLAB deconvolution source code

```
%
% Least squares deconvolution algorithm
% Wim van Cappellen, June 15, 1998.
%
% Based on: Time Domain Deconvolution of Transient Radar Data
%           E.J. Rothwell and W. Sun
%           IEEE Transactions on Antennas and Propagation, April 1990.
%
% In:       yt         measured target response
%           hsys       measured system response
%           threshold  estimated SNR of input signals
%
% Out:      hs         deconvolution of yt and hsys
%

function [hs] = lsdeconv(yt,hsys, threshold)

N=length(hsys);
M=length(yt)-N;
S=zeros(M+N,M);

un(1:(M+N),1)=0;
un(1:N,1)=hsys;
hsys=un;

for i=1:M,
   S(i:(M+N),i)=hsys(1:(M+N-i+1));
end

[u,s,v]=svd(S);
sing=diag(s);
```

```
n=zeros(M,1);

drempel=max(sing)*10^(-threshold/20);

for i = 1:M,
   if sing(i)>drempel
      temp=u'*yt;
      n(i,1)=temp(i)./sing(i);
   else
      n(i,1)=0;
   end
end
hs=v*n;
```

Appendix B

Detailed measurement description

This appendix describes the exact measurement setup and sampling scope settings of the measurements.

B.1 Measurement setup

For all measurements exactly the same cables are used. The pulse generator is connected to the pulse shaper (1) with a 3m Sucoflex cable (from Colarado-project), an N-type to SMA transition and an SMA to N-type transition. The pulse shaper is connected to the transmit antenna with 1m Sucoflex, an N-type to SMA transition, an SMA to N-type transition and an SMA knee (mounted at the antenna side). The receiving antenna is connected to the sample unit with another 3m Sucoflex cable, an N-type to SMA transition and an SMA to N-type transition (from Colarado-project).

For the system response measurement two additional 20dB attenuators were connected between the 3m Sucoflex cable and the sample unit.

B.2 Sampling scope settings

The table below shows the settings of the sampling scope for the system response, object response and the background measurement. The data from this measurement session is stored on the measurement PC in the directory: `C:\USER\DATA\WIM\M260398`.

The rough backside of the object has also been measured. This data is stored in the files `rrpa_8.dat` and `rrpb_8.dat`. The first files contains data of the rotating plate with side A up and the second file contains the results when the plate is mounted with side B up.

	system response	*object response*	*background*
sampletime	20 ps	20 ps	20 ps
# samples	2048	2048	2048
averaging	256	256	256
sensitivity	50 mV/div	50 mV/div	50 mV/div
delay	15.00 ns	2.00 ns	2.00 ns
input channel	2	2	2
filename	dp_8.dat	rfp_8.dat	rbg_8.dat

Appendix C

Literature survey

This appendix shortly describes the interesting features of the references and their relation to this thesis.

C.1 Introduction into time domain (RCS) measurements

These articles, reports and books give a good introduction into several topics concerning time domain RCS measurements.

- *The fundamentals of time domain antenna measurement* [1] and *Time domain antenna measurement report* [2]

  These reports provide a practical introduction into time domain antenna measurements as well as a more theoretical description of the measurements. They also contain a list of interesting references.

- *Antenna time-domain measurement techniques* [3]

  This article gives a description of the IRCTR time domain antenna measurement activities and their results.

- *Radar cross section, its prediction, measurement and reduction* [4]

  This book gives a very good introduction in Radar Cross Section theory, but is also a valuable reference. It contains electromagnetic backgrounds, descriptions of scattering mechanisms and measurement results.

- *Applications of impulse radar technology* [15]

  Modern civil and military applications of impulse radar technology are described in this article.

- *Antenna and radar cross section measurement in the Delft anechoic chamber* [16]

  This thesis provides a description of frequency domain RCS measurements using the facilities at IRCTR. It contains a good description of the frequency domain error sources.

C.2 Detailed background references

- *Antenna characterization in the time domain* [7]

  This article gives a mathematical characterization of antennas which is adopted in this report.

- *Scattering from an artificial rough surface, calculation and measurement* [8]

  This thesis describes the calculations and measurements of an artificial rough surface and its flat backside. This object is also used for the time domain measurements. The results of these measurements and calculations are interesting to compare with the time domain technique.

- *Time domain deconvolution of transient radar data* [9]

  The deconvolution algorith implemented in the signal processing is based on this article. It does not contain a good criterium to select which singular values should be neglected.

- *Comparison of some non-adaptive deconvolution techniques for resolution enhancement of ultrasonic data* [10]

  A selection of well established deconvolution techniques are compared in this article. Both frequency and time domain methods are compared under varying conditions.

- *Deconvolution and total least squares in finding the impulse response of an electromagnetic system from measured data* [12]

  This article describes a total least squares deconvolution algorithm. The article contains a criterium for the threshold which determines which singular values should be neglected.

- *Evaluation of multiple diffraction coefficients using the uniform theory of diffraction* [17]

  This report qualitively and quantitatively describes the multiple diffraction contribution to the scattering of a flat plate in the frequency domain.

C.3 Time domain measurement results in literature

- *Ultra-wideband impulse scattering measurements* [13]

  Description of a wideband time domain scattering laboratory. It contains a short description of the measurement setup, the processing and the results. All processing (background subtraction and range compression) is performed in the frequency domain. The resolution of the results is similar to my resolution. Morgan uses a step pulse (instead of a delta pulse) to perform his measurements.

- *Diffraction of ultrawide band radar pulses* [14]

  This article describes the diffraction contribution to the total scattered field of a flat plate. The resolution of the measurements is relatively low because the bandwidth is very limited (up to 3 GHz). However, the author claims to be able to separate the leading and trailing edge (single diffraction) contributions.

- *Analysis of time domain ultra wideband radar signals* [18]

  This paper outlines analysis techniques for the generation, calibration and processing of ultra wide band time domain radar signals and presents experimental measurements used to illustrate the advantages and disadvantages of such methods.